BRDF-based Irradiance Image Estimation to Remove Radiometric Differences for Stereo Matching

Kebin Peng[a], John Quarles[b] and Kevin Desai[c]
Department of Computer Science, The University of Texas at San Antonio, Texas, U.S.A.

Keywords: Bidirectional Reflectance Distribution Function, Irradiance, Radiometric Differences, Stereo Matching.

Abstract: Existing stereo matching methods assume that the corresponding pixels between left and right views have similar intensity. However, in real situations, image intensity tends to be dissimilar because of the radiometric differences obtained due to change in light reflected. In this paper, we propose a novel approach for removing these radiometric differences to perform stereo matching effectively. The approach estimates irradiance images based on the Bidirectional Reflectance Distribution Function (BRDF) which describes the ratio of radiance to irradiance for a given image. We demonstrate that to compute an irradiance image we only need to estimate the light source direction and the object's roughness. We consider an approximation that the dot product of the unknown light direction parameters follows a Gaussian distribution and we use that to estimate the light source direction. The object's roughness is estimated by calculating the pixel intensity variance using a local window strategy. By applying the above steps independently on the original stereo images, we obtain the illumination invariant irradiance images that can be used as input to stereo matching methods. Experiments conducted on well-known stereo estimation datasets demonstrate that our proposed approach significantly reduces the error rate of stereo matching methods.

1 INTRODUCTION

Estimating depth from stereo image pairs is one of the most fundamental tasks in computer vision (Scharstein and Szeliski, 2002). This task is vital for many applications, such as 3D reconstruction (Geiger et al., 2011), robot navigation and control (Song et al., 2013), object detection and recognition (Chen et al., 2015). The standard approach is to find accurate pixel correspondence and recover the depth using epipolar geometry. Approaches for pixel correspondence work with a color consistency assumption that the pixels in the left and right views have similar color intensity values. However, in real situations, the color intensity values for a given pixel differs between the left and right views. These differences are known as radiometric differences. According to (Heo et al., 2010), light reflection and camera setting changes are two main reasons for having radiometric differences. Light reflection is determined by the angle between the direction of incident ray and the direction of the surface normal (Heo et al., 2010). The same object surface could show a different color intensity value if this angle is different. Another typical situation is the difference in the intensity of the light source. Apart from light reflection, camera settings such as exposure variations decide the amount of light which reaches the camera and hence can also cause differences in the pixel color intensity (Heo et al., 2010).

1.1 Proposed Approach

In this paper, we consider the radiometric differences in stereo images from the viewpoint of the Bidirectional Reflectance Distribution Function (BRDF) (Walter et al., 2007a). Commonly used in Computer Graphics, BRDF considers the micro-structure and light reflection features of an object's surface and describes the ratio of radiance to irradiance for a given image. We propose a novel BRDF-based irradiance image estimation technique for removing radiometric differences. Different from previous approaches (Tan and Triggs, 2010; Han et al., 2013) for radiometric difference removal that focus on radiance, i.e. reflected light from the object's surface, we consider irradiance, i.e. incident light on the object's surface.

Using mathematical foundations around BRDF,

[a] https://orcid.org/0000-0003-4866-786X
[b] https://orcid.org/0000-0002-4790-167X
[c] https://orcid.org/0000-0002-2964-8981

Peng, K., Quarles, J. and Desai, K.
BRDF-based Irradiance Image Estimation to Remove Radiometric Differences for Stereo Matching.
DOI: 10.5220/0010879800003124
In *Proceedings of the 17th International Joint Conference on Computer Vision, Imaging and Computer Graphics Theory and Applications (VISIGRAPP 2022) - Volume 5: VISAPP*, pages 734-744
ISBN: 978-989-758-555-5; ISSN: 2184-4321

(a) Left image (b) Irradiance image of (a)

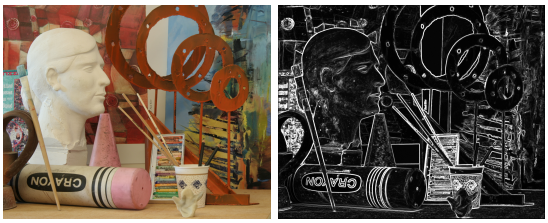

(c) Right image (d) Irradiance image of (c)

Figure 1: ArtL example from Middlebury-14 dataset (Scharstein and Szeliski, 2002) where left (a) and right (b) stereo images have different light conditions. (b) and (d) are the illumination invariant irradiance images corresponding to (a) and (c), that are computed using our radiometric difference removal approach.

we demonstrate that to compute an irradiance image we only need to estimate two parameters - light source direction and object roughness. In our algorithm, we do not need to estimate the unknown light direction parameters separately. Rather only the dot products for these unit direction vectors need to be estimated, for which we employ an approximation strategy based on a Gaussian distribution (see section 3.3). To estimate the surface roughness for the objects in the image, we use a local window approach and estimate the pixel intensity variance (see section 3.4). As the irradiance image is decided by light source intensity and the distance between light sources and objects, it will not be affected by light reflection, viewing angle and camera setting changes (see Figures 6(b) and 1(d)). By using the irradiance image as the input for stereo matching instead of original stereo image pairs, significant performance improvement is obtained for the state-of-the-art stereo matching methods.

1.2 Contributions

In this paper we make the following contributions:

- A Computer Graphics perspective is provided for removing the radiometric differences in stereo images by modeling it with the Bidirectional Reflectance Distribution Function (BRDF).
- Irradiance image estimation is proposed for radiometric difference removal, which is robust to lighting conditions and camera exposure.
- The light source direction is approximated using a Gaussian distribution and object roughness is estimated using local window-based pixel intensity variance.
- Existing stereo matching methods are significantly improved by the use of the estimated irradiance images as opposed to the original left and right stereo images.

2 RELATED WORK

Research in radiometric difference removal can be broadly classified into the following three categories:

2.1 Matching Cost Function

Methods in this category aim at performing stereo matching by proposing matching costs that are robust on images with radiometric differences. Window-based mutual information methods (Egnal, 2000; Fookes et al., 2002; Sarkar and Bansal, 2007) do not require relative ordering and also have similar effectiveness in removing the radiometric differences. Another effective way is to perform segment-wise stereo matching (Zitnick et al., 2004). (Kim et al., 2003) uses mutual information with iterative global graph-cuts to compute matching cost. The hierarchical calculation of pixel-based matching costs, as proposed in (Hirschmuller, 2007), shows the same accuracy results as compared to the window-based approach (Kim et al., 2003). Even though these methods work well in removing radiometric differences, they require a large local-window size to obtain good performance, which results in a high time consumption.

2.2 Pixel Transformation

Pixel transformation methods use a function to remap the pixel intensity in an image, making the pixel intensity values obey a specific distribution or a curve. (Khan et al., 2015) uses normalized histogram to make the pixel intensity values obey a uniform distribution. (Deng, 2016; Changyong et al., 2014) apply log functions on an image to make the pixel intensity values obey a log curve. (Rahman et al., 2016; Deng, 2016) make the pixel intensity values obey a gamma curve by applying gamma correction techniques. These pixel-transformation methods work well only when the background and foreground have similar pixel intensity. Many techniques have been proposed to overcome this drawback. (Zhuang and Guan, 2017) divides the whole image into sub-images and then normalizes each sub-image by its mean and

variance-based histogram. (Campos et al., 2019) proposes a machine-learning based approach for hyper-parameter selection in order to perform a contrast limited adaptive histogram equalization. However, because methods in this category only consider the pixel intensity and ignore the light condition and object material, they have not been able to effectively deal with radiometric differences. Also, because uniform distribution makes pixel intensity similar, histogram methods, such as (Khan et al., 2015), are more likely to create blurry disparity maps.

2.3 Reflectance Estimation

Methods in this category take a more direct approach and estimate the reflectance from a 2D image, which is light invariant when objects have the same reflectivity. Usually, this idea depends on an illumination model, e.g., reflectance-illumination model. (Xie and Lam, 2006) proposes a local normalization method by assuming that objects, faces in their case, consist of a combination of small facets and remove the radiometric differences by performing normalization on these facets. (Tan and Triggs, 2010) proposes local ternary patterns to remove the radiometric differences by using thresholds for neighboring pixels based on the value of the central pixel. While the above two methods estimate reflectance indirectly, (Chen et al., 2006) develops total variation models which consider a 2D image as the product of light source intensity and a kernel function. However, selecting a specific kernel function may not be applicable to images with varying light conditions. Moreover, these methods do not consider the object's micro surface structure which could influence the reflectance.

In this paper, we exploit the advantages of all the above three categories to design a radiometric difference removal algorithm that considers image reflectance for all pixels in a given window. As opposed to matching cost methods, our approach performs a lot faster as it only considers a static-sized window. Compared with existing pixel transformation approaches, our reflectance-based method works on each pixel separately and hence does not result in a blurry disparity map. Our method performs consistently well on images from a variety of well-known stereo matching datasets. Our radiometric difference removal approach is described in Section 3, with the experiments and results reported in Section 4. We further analyze and discuss some of our results in Section 4.7 and provide concluding remarks in Section 5.

3 PROPOSED APPROACH

The overall objective of our approach is to estimate the left and right irradiance images by removing the radiometric differences from the stereo image pairs. Stereo matching is applied on these irradiance images instead of the original stereo images to obtain improved disparity map results. As shown in Figure 2, the proposed radiometric difference removal algorithm consists of three parts: (1) irradiance image computation, (2) light direction estimation, and (3) object roughness estimation.

3.1 Assumptions

A given pixel can receive light from two types of sources - direct light and indirect light. To simplify our model, we assume that there is a single direct light source following other BRDF estimation papers, e.g., (Chung et al., 2006) and we call it *single light source assumption*. Indirect light refers to the reflected light between objects (ambient light). We

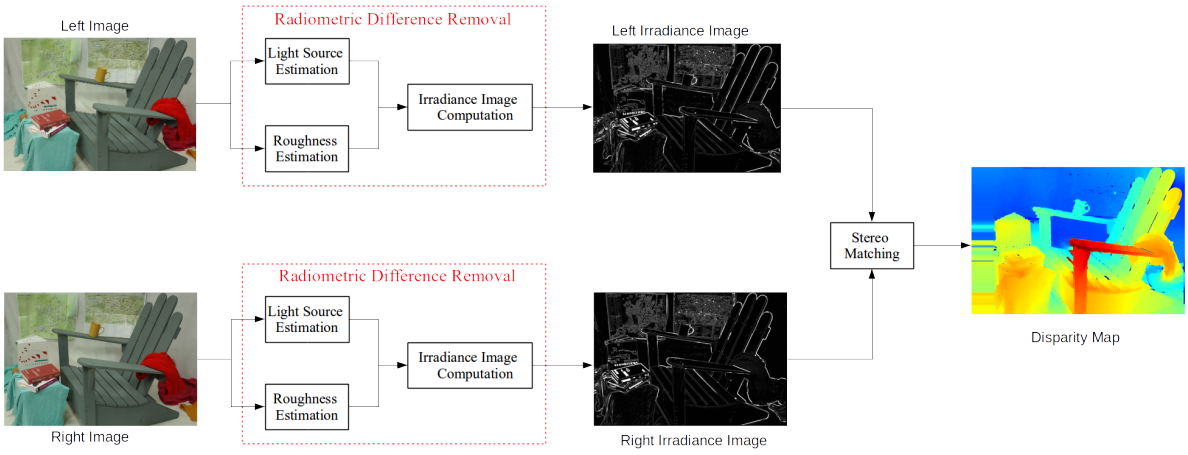

Figure 2: Overview of the proposed radiometric difference removal approach for Stereo Matching.

further assume that ambient light comes from all directions except light source direction with nearly the same lighting brightness and we call it *uniform ambient light assumption*. With such assumptions, we use order-0 Spherical Harmonics to model the ambient light (Sloan et al., 2005).

3.2 Irradiance Image Computation

BRDF, denoted by $f_r(\mathbf{i},\mathbf{o})$, is the ratio of scattered radiance $L(\mathbf{i})$ in the direction i to irradiance $E(\mathbf{o})$ from the direction o. Based on this definition, we perform irradiance image estimation using the equation:

$$E(\mathbf{o}) = \frac{L(\mathbf{i})}{f_r(\mathbf{i},\mathbf{o})} \tag{1}$$

Using Microfacet theory, (Walter et al., 2007b) shows that a roughness term α can be incorporated into BRDF for describing an object's micro-surface. By applying that formulation to our Equation 1, we obtain the following:

$$E(\mathbf{o}) = \int_{i\in\Omega} \frac{L(\mathbf{i})4\,|\mathbf{i}\cdot\mathbf{n}|\,|\mathbf{o}\cdot\mathbf{n}|}{F_{schlick}(F_0,\mathbf{h},\mathbf{i})\,G(\mathbf{n},\mathbf{o},\alpha)\,D(\mathbf{h})} \tag{2}$$

The integral in the above equation represents all possible incoming light for the pixel in the upper hemisphere (Ω in Equation 3). $\mathbf{i}$ is the direction of the reflected light from an object's surface. $\mathbf{o}$ is the direction of light coming from the light source. $\mathbf{n}$ refers to the direction of the object surface's normal. $\mathbf{h}$ is the normalized half-vector of $\mathbf{i}$ and $\mathbf{o}$. $F(\mathbf{i},\mathbf{h})$ is a Fresnel term which describes the reflection and transmission of light when incident on an interface between different optical media. It is usually approximated using Fresnel-Schlick function $F_{schlick}(F_0,\mathbf{h},\mathbf{i})$ (Schlick, 1994) where F_0 is the reflection coefficient for light incoming parallel to the normal. $G(\mathbf{i},\mathbf{o},\alpha)$ is the Geometrical Attenuation Factor (Kelemen and Szirmay-Kalos, 2001) which describes what percentage of the reflected light will not be blocked by the surface topography (Hao et al., 2019). $D(\mathbf{h})$ is the GGX Distribution Function (Walter et al., 2007a) which describes the probability distribution of the surface normal.

To solve Equation 3, we first discuss the possible incoming light directions in the upper hemisphere for a pixel. According to *single light source assumption* in Section 3.1, the direct light only has one direction, which is the light source direction. However, the indirect light has unlimited directions in the upper hemisphere. Here, we apply *uniform ambient light assumption*, as mentioned in Section 3.1. That is, the ambient light comes in all directions except light source direction with nearly the same lighting brightness. So the ambient can be viewed as a constant C. Intuitively, We may set C as the mean value of input images, or we could use 0-order Spherical Harmonics function (Sloan et al., 2005), which is $\sqrt{\frac{1}{4\pi}}$, to model the ambient light. So Equation 3 can be simplified as:

$$E(\mathbf{o}) = \frac{L(\mathbf{i})4\,|\mathbf{i}\cdot\mathbf{n}|\,|\mathbf{o}\cdot\mathbf{n}|}{F_{schlick}(F_0,\mathbf{h},\mathbf{i})\,G(\mathbf{n},\mathbf{o},\alpha)\,D(\mathbf{h})} + C \tag{3}$$

Next, we estimate the reflected light $L(\mathbf{i})$ as received by the camera by mapping it to image pixel intensity. This is modeled by the camera response function which, according to (Ng et al., 2007), is assumed to be a gamma curve that is generally approximated by a polynomial function. We compared different types of polynomial approximations (linear, quadratic, etc.) and found no significant difference between them. Hence, in our approach we approximate the camera response function using a linear function which implies that $L(\mathbf{i})$ is the same as image intensity.

After solving for $L(\mathbf{i})$, the only unknown variables that need to be estimated are $\mathbf{i}$, $\mathbf{o}$, $\mathbf{n}$, $\mathbf{h}$, and α. The first four parameters are associated with the light direction, whereas the last parameter is the object surface roughness. Considering theoretical foundations and expansion of the functions in Equation 3, parameters $\mathbf{i}$, $\mathbf{o}$, $\mathbf{n}$, and $\mathbf{h}$ are never used on their own. Rather, they are always used in combinations as a dot product. In Section 3.3, we demonstrate that the dot product of any of these parameters obeys a Gaussian distribution, based on which we estimate the light direction. We estimate the surface roughness α using a local window-based approach for pixel intensity variance, shown in Section 3.4.

3.3 Light Direction Estimation

As mentioned above, light source direction can be estimated by approximating the dot products of $\mathbf{i}$, $\mathbf{o}$, $\mathbf{n}$, and $\mathbf{h}$. We demonstrate that any combination of the dot products of these direction vectors follow a Gaussian distribution.

Assume $\mathbf{a}$ and $\mathbf{b}$ are any of the four direction vectors $\mathbf{i}$, $\mathbf{o}$, $\mathbf{n}$, and $\mathbf{h}$. The dot product of $\mathbf{a}$ and $\mathbf{b}$ can be represented as $\mathbf{a}\cdot\mathbf{b} = |\mathbf{a}|\,|\mathbf{b}|\cos\theta$. These vectors are normalized unit direction vectors. Hence, the dot product is dependent on just the cosine of the angle θ between a and b i.e. $\cos\theta$. As we do not know the angle between these vectors, we cannot find the value for $\cos\theta$. Considering that $\theta \in [-\pi,\pi]$, by selecting specific values for μ and σ^2, we can plot the function graph for the Gaussian distribution $N(\mu,\sigma^2)$. Visual comparison shows that this Gaussian function graph is very similar to the function graph for $\cos\theta$. Hence,

we use Gaussian distribution to approximate the value for $\cos\theta$.

In Equation 3, we estimate the irradiance value for each pixel of an image of length l and height h. We need to obtain a specific dot product value for the four direction vectors **i**, **o**, **n**, and **h**. Hence, we generate a Gaussian distribution $N(\mu,\sigma^2)$ for $l*h$ values and pick the value that matches the row and column value for the corresponding image. This value is used for the light source direction estimation.

3.4 Roughness Estimation

As mentioned in Section 3.2, we need to estimate the object surface roughness α in order to compute the irradiance images. Surface element roughness describes how flat (low roughness) or how rugged (high roughness) a surface is at a micro level. It is dependent on the object's material and is usually set manually according to a visual understanding of the object in the image. However, in stereo image pairs consisting of multiple objects, it is not possible to effectively set an appropriate value manually.

According to BRDF (Walter et al., 2007a), surface roughness has an inverse relationship with local pixel intensity variance. If the object surface has high roughness, the reflected light would be more likely to be scattered into different directions. This difference in light direction could make the image seem blurry indicating that it has smaller pixel intensity variance. We design a local window-based approach to approximate the pixel intensity variance which leads to the estimation of surface roughness α based on the following equation:

$$\alpha = \frac{1}{V_t(p)} = \frac{1}{\sum_{i=1}^{t}\sum_{j=1}^{t}(p_{ij} - M_t(p))^2} \quad (4)$$

where p is the center pixel for which we are trying to estimate the pixel intensity variance $V_t(p)$ in a local square window of size t (an odd number). $M_t(p)$ denotes the mean pixel intensity value in this window.

Based on the approach mentioned above in Sections 3.2, 3.3, and 3.4, we compute the left and right irradiance images for the original stereo image pairs. The radiometric differences are removed in these irradiance images which can then be applied to any stereo matching method.

4 EXPERIMENTS

In this section, we conduct extensive experimental analysis to evaluate the effectiveness of our radiometric difference removal algorithm on stereo matching.

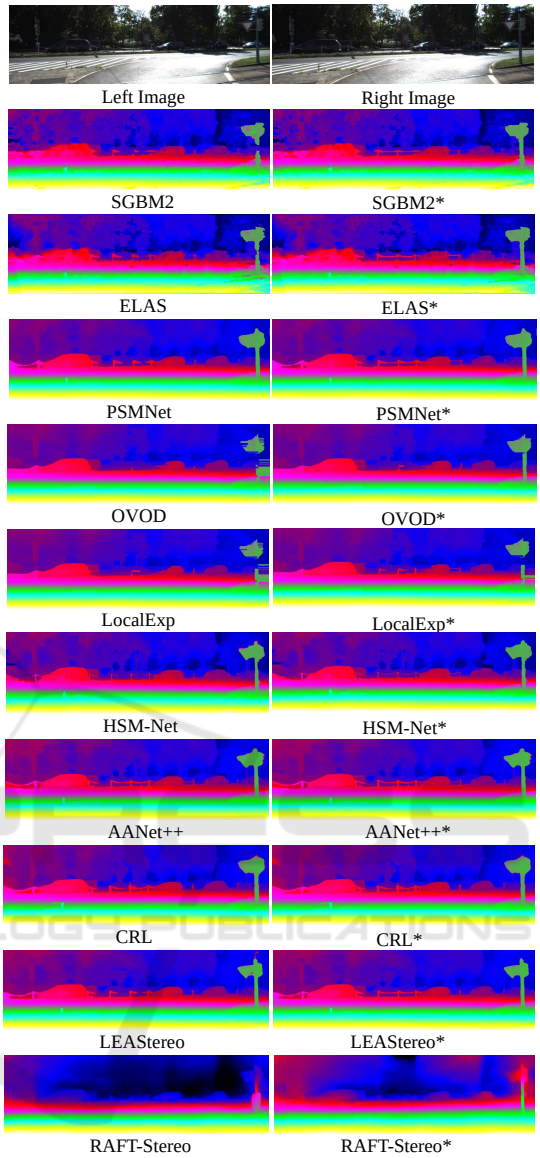

Figure 3: An example image from the test set (so no ground truth) of KITTI-15 dataset (Scharstein et al., 2014). * denotes the use of our approach prior to applying the stereo matching methods.

4.1 Implementation Details

All the experiments are conducted on a computer having a 2.6 GHz CPU with an i7 processor and 32 GB RAM. Our radiometric removal algorithm for converting the original stereo images to irradiance images is implemented in C++. For the Fresnel-Schlick function (Schlick, 1994) used in Equation 3, we use linear base reflectivity and set $F_0 = 0.365$. We conducted a separate experiment and found that there were no major differences in our results across different F_0 values. We picked the value which gave

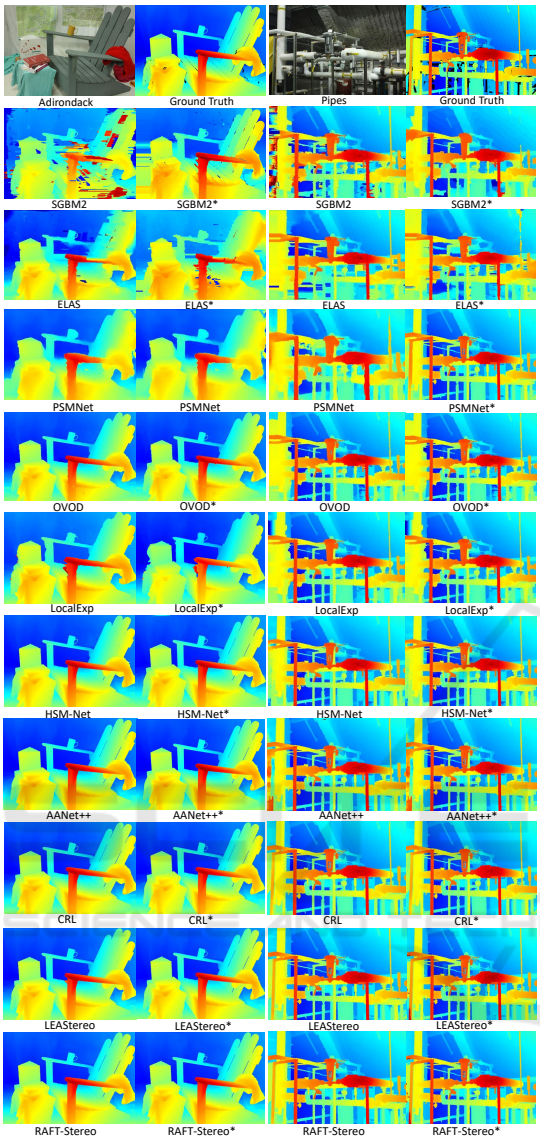

Figure 4: Adirondack image and Pipes image from the Middlebury-14 dataset (Scharstein et al., 2014) along with the ground truth disparity map. First and third columns show the disparity maps generated by 10 stereo matching methods on the original stereo image pairs. Second and fourth columns show results on the irradiance images estimated by our radiometric difference removal algorithm (denoted by *).

the best results. We did the same for the Gaussian distribution $N(\mu,\sigma^2)$ parameters and set them to be $\mu = 10$ and $\sigma = 1$. The Gaussian distribution is then used as an approximation of $\cos\theta$ in estimating the light direction (see Section 3.3). In Equation 4 we select the local square window size to be $t = 5$ because we find that it results in the best performance. Also, we set ambient light constant $C = \sqrt{\frac{1}{4\pi}}$ as it yields better results. Implementation details of the different stereo matching methods we use in our experiments are mentioned in Section 4.3.

4.2 Datasets & Evaluation Metrics

We use three popular stereo matching datasets and the corresponding evaluation metrics.

- Middlebury-14 (Scharstein et al., 2014) is a high-resolution two-view dataset that consist of multiple stereo images of indoor scenes. We use the 15 training stereo image pairs and focus only on the non-occluded pixels during evaluation. *avgerr*, *bad-0.5*, *bad-1.0*, and *bad-2.0* are used as the evaluation metrics for this dataset.
- Middlebury-06 (Hirschmuller and Scharstein, 2007) is the older version of the Middlebury-14 dataset. We use this to evaluate our method against other pre-processing methods in different lighting and exposure conditions. We use the *avgerr* metric to graph the comparisons.
- KITTI-15 (Menze et al., 2018) dataset is also used to evaluate the impact of our proposed pre-processing method on other stereo matching methods. We perform analysis on all the 200 low resolution stereo pairs. The metrics used for this dataset are *D1-all*, *D1-bg* and *D1-fg*, which refer to the percentage of outliers for all pixels, background pixels, and foreground pixels respectively.

For all experiments, we use * to denote the use of our radiometric removal algorithm with the corresponding stereo matching method or evaluation metric.

4.3 Stereo Matching Estimation Methods Compared

Several pre-processing optimization approaches exist for improving stereo matching, such as (Heo et al., 2012) and (Zhou and Boulanger, 2012), which are illumination invariant approaches. However, these approaches also change the cost function and hence cannot directly be compared with our approach. Radiometric invariant filters such as gradient, census, and rank filters can also be used for optimizing stereo matching. These filters also depend on the cost function. On the other hand, our approach is separate from the cost function. This is the major advantage of our method that it can work with any stereo matching algorithms using their individual cost functions.

The irradiance images obtained from our radiometric removal algorithm are used as input for 10 representative state-of-the-art stereo matching methods: SGBM2 (Hirschmuller, 2007), ELAS (Geiger

et al., 2010), AANet++ (Xu and Zhang, 2020), PSMNet (Chang and Chen, 2018), HSM-Net (Yang et al., 2019), LEAStereo (Cheng et al., 2020),LocalExp (Taniai et al., 2017), OVOD (Mozerov and van de Weijer, 2019),CRL (Pang et al., 2017), RAFT-Stereo (Lipson et al., 2021). For Figure 4 shows the disparity maps for the Adirondack image and Pipes image in the Middlebury-14 dataset. For all methods, except SGBM2, we directly use implementations available online on their respective GitHub repositories. However, we do need to fine-tune specific parameters in their models to obtain the reported results on different datasets. We implement SGBM2 (Hirschmuller, 2007) using OpenCV by setting the following parameter values to accurately replicate results: SAD window size = 3, truncation value for prefilter = 63, P1 = $8*3*3$, P2 = $32*3*3$, uniqueness ratio = 10, speckle window size = 100, speckle range = 32, max disparity value = 128. We also set the input image resolution to be half of the original.

Here, we perform experimental analysis on each of the four datasets and report the results for the same. **Middlebury-14 Dataset (Scharstein et al., 2014):** Figure 4 shows visual disparity map results for the Adirondack image from the Middlebury-14 dataset (Scharstein et al., 2014). As visible in the disparity maps, the results obtained on the stereo matching methods after applying our radiometric removal algorithm (bottom row) are better compared to the ones obtained without using our algorithm (top row). The dataset consists of 15 stereo image pair test cases on which we conduct our analysis. We conduct experiments for all 10 stereo matching methods on these image pairs using avgerr, bad-0.5, bad-1.0, and bad-2.0 as the evaluation metrics.

Table 1 shows the results for our experimental analysis. In the majority of the cases, we obtain a reduction in the error rates indicating the effectiveness of our algorithm for stereo matching. For example, we obtain avgerr reduction of 34.43% for SGBM2 and 6.12% for AANet++. The worst performance is for HSM-Net where avgerr increases by 1.41%.

KITTI-15 Dataset (Menze et al., 2018): We report results for all the three percentages of outliers metrics that are generally used for this dataset - *D1-all*, *D1-bg*, and *D1-fg*. Table 2 shows the results for all the 10 stereo matching methods with and without the use of our algorithm. As shown in the table, by using our algorithm, all methods report performance improvement across all metrics. For example, for D1-all, error reduction is obtained in the range of $1.05\% - 37.99\%$. Figure 3 shows visual disparity map results for an example image from the test set in KITTI-15 Dataset.

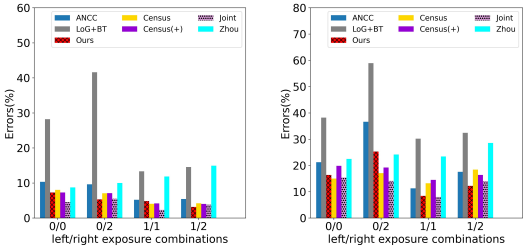

(a) Aloe (b) Art

Figure 5: Comparison of our approach with other pre-processing approaches for camera exposure changes on three images from the Middlebury-06 dataset (Hirschmuller and Scharstein, 2007).

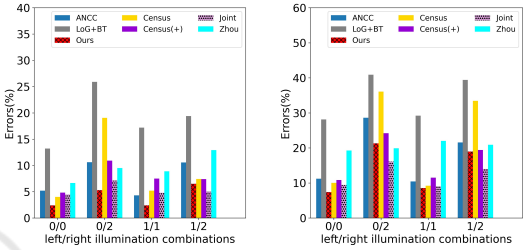

(a) Aloe (b) Art

Figure 6: Comparison of our approach with other pre-processing approaches for changes in the light source on three images from the Middlebury-06 dataset (Hirschmuller and Scharstein, 2007).

4.4 Robustness to Camera Exposure & Light Source Changes

We also evaluate the robustness of our approach across different camera exposure settings as well as changes to the light source. We use two different images from the Middlebury-06 dataset (Hirschmuller and Scharstein, 2007) to compare our approach with the five other pre-processing approaches. For this analysis, we use the same experimental setting as in the ANCC work (Heo et al., 2008). Also, same as in (Heo et al., 2012), we have included Census(+) in our evaluation which uses a combined log-chromaticity color (70% weight) and RGB color (30% weight).

Figure 5 shows the two comparison graphs with each having four different camera exposure combinations between the left and the right views. Similarly, Figure 6 shows the comparison graphs for light source changes. As seen from the graphs, our approach outperforms most other pre-processing approaches in all the four combinations for left/right views, for both camera exposure and light source changes.

Table 1: Results on the Middlebury-14 (Scharstein et al., 2014) training set for 10 stereo matching methods (our algorithm denoted by *). Percentage change in the error values is shown in parenthesis with an arrow indicating increase or decrease.

Method	Res	avgerr	avgerr*	bad-0.5	bad-0.5*	bad-1.0	bad-1.0*	bad-2.0	bad-2.0*
SGBM2	F	11.15	7.31 (34.43%↓)	56.71	38.60 (31.93%↓)	36.18	24.43 (32.4%↓)	27.52	23.57 (14.35%↓)
ELAS	F	7.56	7.62 (0.79%↑)	61.62	60.58 (1.68%↓)	38.73	37.27 (0.65%↓)	27.88	26.18 (0.93%↓)
PSMNet	Q	9.92	9.87 (0.50%↓)	89.98	98.90 (9.91%↑)	78.34	77.83 (3.76%↓)	59.11	58.56 (6.09%↓)
OVOD	H	1.82	1.79 (1.64%↓)	38.22	37.81 (1.07%↓)	17.91	17.75 (0.89%↓)	9.67	9.53 (1.44%↓)
LocalExp	H	1.76	1.74 (1.13%↓)	38.45	38.17 (0.72%↓)	14.32	14.20 (0.83%↓)	6.43	6.31 (1.86%↓)
HSM-Net	F	1.41	1.43 (1.41%↑)	50.29	49.61 (1.35%↓)	22.99	23.24 (1.08%↑)	10.78	10.83 (0.46% ↑)
CRL	H	1.45	1.43(1.38%↓)	47.35	46.18(2.47%↓)	19.53	19.19(1.74%↓)	12.71	12.54(1.33%↓)
RAFT-Stereo	H	1.04	0.98(5.76%↓)	28.61	25.42(11.1%↓)	10.60	10.12(4.52%↓)	5.25	4.92(6.28%↓)
LEAStereo	H	1.09	1.03 (5.5%↓)	36.10	35.71 (1.08%↓)	18.40	17.91 (2.7%↓)	2.47	2.52 (2.02% ↑)
AANet++	H	0.98	0.92 (6.12%↓)	33.18	31.95 (3.70%↓)	12.18	11.49 (5.66%↓)	5.65	5.09 (9.91%↓)

Table 2: Results on the KITTI-15 dataset (Menze et al., 2018) with D1-all, D1-bg, and D1-fg evaluation metrics. Superscript (e.g., D1-all*) denotes the use of our algorithm prior to applying the stereo matching methods. Percentage change in the error values is shown in parenthesis with an arrow indicating increase or decrease.

Method	D1-all	D1-all*	D1-bg	D1-bg*	D1-fg	D1-fg*
SGBM2	6.87	4.26 (37.99%↓)	15.29	11.68 (23.61%↓)	5.15	4.27 (17.08%↓)
ELAS	9.78	8.14 (16.85%↓)	19.04	14.93 (21.58%↓)	7.86	5.42 (31.04%↓)
PSMNet	2.32	2.24 (3.44%↓)	1.88	1.64 (12.36%↓)	4.65	4.39 (5.59%↓)
OVOD	4.21	3.9 (7.36%↓)	3.21	3.23 (0.62%↑)	5.94	5.28 (11.11%↓)
LocalExp	4.76	4.71 (1.05%↓)	3.52	3.78 (7.38%↑)	7.47	6.21 (16.86%↓)
HSM-Net	2.19	2.05 (6.39%↓)	1.82	1.76 (3.29%↓)	3.86	3.71 (3.88%↓)
CRL	2.15	2.14(0.46%↓)	2.25	2.21(1.77%↓)	3.41	3.43(0.58%↑)
RAFT-Stereo	1.96	1.73(11.7%↓)	1.75	1.66(5.14%↓)	2.89	2.69 (6.92%↓)
LEAStereo	1.65	1.73 (3.03%↑)	1.40	1.43(2.14 %↑)	2.91	2.93 (0.69%↑)
AANet++	2.31	2.02 (12.55%↓)	2.10	1.94 (7.61%↓)	5.35	5.22 (2.43%↓)

Table 3: Comparison of our approach with five other pre-processing approaches when used in conjunction with all the 10 stereo matching methods. We report the average error obtained on the Middlebury-14 dataset (Scharstein et al., 2014). Best result is marked in bold.

Method	No Pre-processing	Ours	Census	LoG	ANCC	Joint	Zhou
SGBM2	11.5	**7.31**	7.96	9.15	15.81	12.64	16.72
ELAS	7.56	7.62	13.06	15.54	7.16	**7.14**	22.58
PSMNet	9.92	9.87	12.24	12.63	8.40	**7.28**	18.63
OVOD	1.82	1.79	1.93	2.65	**1.73**	1.75	5.11
LocalExp	1.76	**1.74**	2.24	3.43	2.28	2.30	9.98
HSM-Net	1.41	1.43	**1.39**	4.34	2.45	2.43	7.52
CRL	1.45	**1.43**	1.47	4.69	2.72	2.30	6.85
RAFT-Stereo	1.04	**0.98**	1.52	1.31	1.49	1.23	1.77
LEAStereo	1.09	**1.03**	2.02	1.89	3.15	3.37	3.95
AANet++	0.98	**0.92**	1.49	4.07	3.65	3.43	4.84

4.5 Comparison with Other Pre-processing Methods

As ours is a pre-processing method, we also compare it with five other pre-processing methods that use radiometric invariant filters, namely ANCC (Heo et al., 2008) that uses Chromaticity normalization, Laplacian of Gaussian (LoG) + BT (Birchfield and Tomasi, 1998), Census (7×7) (Zabih and Woodfill, 1994) + Hamming, Joint (Heo et al., 2012) that uses Log Chromaticity normalization, and Zhou (Zhou and Boulanger, 2012) that uses Relative Gradients. Because our approach is separate from the stereo matching algorithm, we use BT (Birchfield and Tomasi, 1998) as our stereo matching algorithm for fair comparison. We use GraphCut (GC) to optimize all the matching costs as the same as (Heo et al., 2012).

In Table 3, we report the avgerr results for ours and each of the five other pre-processing approaches when used in conjunction with the 10 state-of-the-

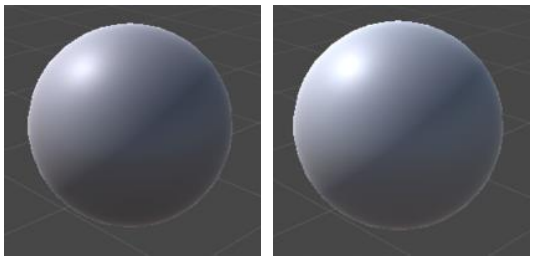

(a) Origianl Sphare (b) Simulated Sphare

Figure 7: Comparison of our original image and our re-rendered image. (a) is rendered with the original BRDF model (b) is re-rendered with our estimated BRDF value.

art stereo matching algorithms. As seen from the results, our approach improves the performance by reducing the errors significantly for all 10 stereo matching methods, as opposed to the other pre-processing approaches that use radiometric invariant filters.

4.6 Validation of BRDF Estimation

We evaluated the accuracy of BRDF estimation using a simulated image, as it is difficult to obtain the actual BRDF ground truth values. We first use Unity3 to render the original image (a) with our own BRDF shader, so the ground-truth BRDF values are known. Then we use our proposed approach to estimate the BRDF for image (a). At last, we use this estimated BRDF to render a new reconstructed image, which we compare with the original image. Figure 7 shows the results for two different images where we compare the original (a) and the simulated images (b) to visually validate the accuracy of the proposed BRDF estimation approach.

4.7 Limitations & Future Work

Our approach for irradiance image computation estimates the light source direction statistically. So there is a difference between our estimated value and the real value for the light source direction. We will investigate such differences in the future. In general Computer Graphics, the lighting function is preknown and can be used to estimate the ambient light. However, in our approach the lighting function is unknown. Hence, we plan to investigate the estimation of the ambient light constant C by using Monte Carlo Sampling Methods in the future.

5 CONCLUSIONS

In this paper we propose a novel radiometric difference removal algorithm for improving the performance of stereo matching methods. The approach is based on the Computer Graphics concept of BRDF to compute the irradiance images for the original left and right stereo images. For doing so, we estimate the light source direction by considering an approximation that the dot product of the unknown light direction parameters follows a Gaussian distribution. We estimate the object's roughness by employing a local window strategy and calculating the pixel intensity variance. The obtained irradiance images are robust to changes in illumination, exposure, and light source intensity. These images when used as input for stereo matching methods improve the quality of the generated disparity maps as opposed to the ones obtained while running the methods on the original stereo images. Results on the experiments performed on 10 stereo matching methods show significant performance improvement for disparity map generation.

REFERENCES

Birchfield, S. and Tomasi, C. (1998). A pixel dissimilarity measure that is insensitive to image sampling. *IEEE Transactions on Pattern Analysis and Machine Intelligence*, 20(4):401–406.

Campos, G. F. C., Mastelini, S. M., Aguiar, G. J., Mantovani, R. G., de Melo, L. F., and Barbon, S. (2019). Machine learning hyperparameter selection for contrast limited adaptive histogram equalization. *EURASIP Journal on Image and Video Processing*, 2019(1):59.

Chang, J.-R. and Chen, Y.-S. (2018). Pyramid stereo matching network. In *Proceedings of the IEEE Conference on Computer Vision and Pattern Recognition*, pages 5410–5418.

Changyong, F., Hongyue, W., Naiji, L., Tian, C., Hua, H., Ying, L., et al. (2014). Log-transformation and its implications for data analysis. *Shanghai archives of psychiatry*, 26(2):105.

Chen, T., Yin, W., Zhou, X. S., Comaniciu, D., and Huang, T. S. (2006). Total variation models for variable lighting face recognition. *IEEE transactions on pattern analysis and machine intelligence*, 28(9):1519–1524.

Chen, X., Kundu, K., Zhu, Y., Berneshawi, A. G., Ma, H., Fidler, S., and Urtasun, R. (2015). 3d object proposals for accurate object class detection. In *Advances in Neural Information Processing Systems*, pages 424–432.

Cheng, X., Zhong, Y., Harandi, M., Dai, Y., Chang, X., Li, H., Drummond, T., and Ge, Z. (2020). Hierarchical neural architecture search for deep stereo matching. *Advances in Neural Information Processing Systems*, 33.

Chung, A. J., Deligianni, F., Shah, P., Wells, A., and Yang, G.-Z. (2006). Patient-specific bronchoscopy visualization through brdf estimation and disocclusion correction. *IEEE transactions on medical imaging*, 25(4):503–513.

Deng, G. (2016). A generalized gamma correction algorithm based on the slip model. *EURASIP Journal on Advances in Signal Processing*, 2016(1):69.

Egnal, G. (2000). Mutual information as a stereo correspondence measure.

Fookes, C., Bennamoun, M., and Lamanna, A. (2002). Improved stereo image matching using mutual information and hierarchical prior probabilities. In *Object recognition supported by user interaction for service robots*, volume 2, pages 937–940. IEEE.

Geiger, A., Roser, M., and Urtasun, R. (2010). Efficient large-scale stereo matching. In *Asian conference on computer vision*, pages 25–38. Springer.

Geiger, A., Ziegler, J., and Stiller, C. (2011). Stereoscan: Dense 3d reconstruction in real-time. In *2011 IEEE intelligent vehicles symposium (IV)*, pages 963–968. Ieee.

Han, H., Shan, S., Chen, X., and Gao, W. (2013). A comparative study on illumination preprocessing in face recognition. *Pattern Recognition*, 46(6):1691–1699.

Hao, D., Wen, J., Xiao, Q., You, D., and Tang, Y. (2019). An improved topography-coupled kernel-driven model for land surface anisotropic reflectance. *IEEE Transactions on Geoscience and Remote Sensing*.

Heo, Y. S., Lee, K. M., and Lee, S. U. (2008). Illumination and camera invariant stereo matching. In *2008 IEEE Conference on Computer Vision and Pattern Recognition*, pages 1–8. IEEE.

Heo, Y. S., Lee, K. M., and Lee, S. U. (2010). Robust stereo matching using adaptive normalized cross-correlation. *IEEE Transactions on Pattern Analysis and Machine Intelligence*, 33(4):807–822.

Heo, Y. S., Lee, K. M., and Lee, S. U. (2012). Joint depth map and color consistency estimation for stereo images with different illuminations and cameras. *IEEE transactions on pattern analysis and machine intelligence*, 35(5):1094–1106.

Hirschmuller, H. (2007). Stereo processing by semiglobal matching and mutual information. *IEEE Transactions on pattern analysis and machine intelligence*, 30(2):328–341.

Hirschmuller, H. and Scharstein, D. (2007). Evaluation of cost functions for stereo matching. In *2007 IEEE Conference on Computer Vision and Pattern Recognition*, pages 1–8. IEEE.

Kelemen, C. and Szirmay-Kalos, L. (2001). A microfacet based coupled specular-matte brdf model with importance sampling. In *Eurographics short presentations*, volume 25, page 34.

Khan, M. F., Khan, E., and Abbasi, Z. (2015). Image contrast enhancement using normalized histogram equalization. *Optik*, 126(24):4868–4875.

Kim, J. et al. (2003). Visual correspondence using energy minimization and mutual information. In *Proceedings Ninth IEEE International Conference on Computer Vision*, pages 1033–1040. IEEE.

Lipson, L., Teed, Z., and Deng, J. (2021). Raft-stereo: Multilevel recurrent field transforms for stereo matching. *arXiv preprint arXiv:2109.07547*.

Menze, M., Heipke, C., and Geiger, A. (2018). Object scene flow. *ISPRS Journal of Photogrammetry and Remote Sensing (JPRS)*.

Mozerov, M. G. and van de Weijer, J. (2019). One-view occlusion detection for stereo matching with a fully connected crf model. *IEEE Transactions on Image Processing*, 28(6):2936–2947.

Ng, T.-T., Chang, S.-F., and Tsui, M.-P. (2007). Using geometry invariants for camera response function estimation. In *2007 IEEE Conference on Computer Vision and Pattern Recognition*, pages 1–8. IEEE.

Pang, J., Sun, W., Ren, J. S., Yang, C., and Yan, Q. (2017). Cascade residual learning: A two-stage convolutional neural network for stereo matching. In *Proceedings of the IEEE International Conference on Computer Vision Workshops*, pages 887–895.

Rahman, S., Rahman, M. M., Abdullah-Al-Wadud, M., Al-Quaderi, G. D., and Shoyaib, M. (2016). An adaptive gamma correction for image enhancement. *EURASIP Journal on Image and Video Processing*, 2016(1):1–13.

Sarkar, I. and Bansal, M. (2007). A wavelet-based multiresolution approach to solve the stereo correspondence problem using mutual information. *IEEE Transactions on Systems, Man, and Cybernetics, Part B (Cybernetics)*, 37(4):1009–1014.

Scharstein, D., Hirschmüller, H., Kitajima, Y., Krathwohl, G., Nešić, N., Wang, X., and Westling, P. (2014). High-resolution stereo datasets with subpixel-accurate ground truth. In *German conference on pattern recognition*, pages 31–42. Springer.

Scharstein, D. and Szeliski, R. (2002). A taxonomy and evaluation of dense two-frame stereo correspondence algorithms. *International journal of computer vision*, 47(1-3):7–42.

Schlick, C. (1994). An inexpensive brdf model for physically-based rendering. In *Computer graphics forum*, volume 13, pages 233–246. Wiley Online Library.

Sloan, P.-P., Luna, B., and Snyder, J. (2005). Local, deformable precomputed radiance transfer. *ACM Transactions on Graphics (TOG)*, 24(3):1216–1224.

Song, D.-l., Jiang, Q.-l., Sun, W.-c., et al. (2013). A survey: Stereo based navigation for mobile binocular robots. In *Robot Intelligence Technology and Applications 2012*, pages 1035–1046. Springer.

Tan, X. and Triggs, B. (2010). Enhanced local texture feature sets for face recognition under difficult lighting conditions. *IEEE transactions on image processing*, 19(6):1635–1650.

Taniai, T., Matsushita, Y., Sato, Y., and Naemura, T. (2017). Continuous 3d label stereo matching using local expansion moves. *IEEE transactions on pattern analysis and machine intelligence*, 40(11):2725–2739.

Walter, B., Marschner, S. R., Li, H., and Torrance, K. E. (2007a). Microfacet models for refraction through rough surfaces. In *Proceedings of the 18th Eurographics Conference on Rendering Techniques*, EGSR'07, page 195–206, Goslar, DEU. Eurographics Association.

Walter, B., Marschner, S. R., Li, H., and Torrance, K. E. (2007b). Microfacet models for refraction through rough surfaces. *Rendering techniques*, 2007:18th.

Xie, X. and Lam, K.-M. (2006). An efficient illumination normalization method for face recognition. *Pattern Recognition Letters*, 27(6):609–617.

Xu, H. and Zhang, J. (2020). Aanet: Adaptive aggregation network for efficient stereo matching. In *Proceedings of the IEEE/CVF Conference on Computer Vision and Pattern Recognition*, pages 1959–1968.

Yang, G., Manela, J., Happold, M., and Ramanan, D. (2019). Hierarchical deep stereo matching on high-resolution images. In *Proceedings of the IEEE Conference on Computer Vision and Pattern Recognition*, pages 5515–5524.

Zabih, R. and Woodfill, J. (1994). Non-parametric local transforms for computing visual correspondence. In *European conference on computer vision*, pages 151–158. Springer.

Zhou, X. and Boulanger, P. (2012). Radiometric invariant stereo matching based on relative gradients. In *2012 19th IEEE International Conference on Image Processing*, pages 2989–2992. IEEE.

Zhuang, L. and Guan, Y. (2017). Image enhancement via subimage histogram equalization based on mean and variance. *Computational intelligence and neuroscience*, 2017.

Zitnick, C. L., Kang, S. B., Uyttendaele, M., Winder, S., and Szeliski, R. (2004). High-quality video view interpolation using a layered representation. *ACM transactions on graphics (TOG)*, 23(3):600–608.